

Collisional mixing among the $z\ 3\ D\ J$ and $z\ 3\ F\ J$ states of Fe atoms in He and Ar

J. S. Goo, K. Lee, S. C. Bae, and J. K. Ku

Citation: *The Journal of Chemical Physics* **105**, 7485 (1996); doi: 10.1063/1.472575

View online: <http://dx.doi.org/10.1063/1.472575>

View Table of Contents: <http://scitation.aip.org/content/aip/journal/jcp/105/17?ver=pdfcov>

Published by the [AIP Publishing](#)

Articles you may be interested in

Collisionenergy/electronenergy resolved twodimensional study of Penning ionization of Ar by He metastable atoms $23\ S$ and $21\ S$

J. Chem. Phys. **105**, 7536 (1996); 10.1063/1.472579

Destruction cross sections for low energy collisions of $H^+\ 3$ and $D^+\ 3$ with rare gas atoms

J. Chem. Phys. **104**, 6149 (1996); 10.1063/1.471280

Collisional energy spread in hotatom reactions caused by thermal motions of the reagents

AIP Conf. Proc. **216**, 301 (1990); 10.1063/1.39925

Satellite of forbidden line Ar ($4s3P2-1S0$) induced by collisions with helium atoms

AIP Conf. Proc. **216**, 287 (1990); 10.1063/1.39919

Noble gas induced collisional line broadening of atomic Li Rydberg states nS and nD ($n=4$ to 30) measured by trilevel echoes

AIP Conf. Proc. **146**, 439 (1986); 10.1063/1.35714



Collisional mixing among the z^3D_J and z^3F_J states of Fe atoms in He and Ar

J. S. Goo, K. Lee, S. C. Bae, and J. K. Ku

Department of Chemistry, Pohang University of Science and Technology, San 31 Hyoja-Dong, Pohang, Kyungbuk 790-784, Korea

(Received 6 May 1996; accepted 24 July 1996)

Collisional mixing among the z^3D_J and z^3F_J states of Fe[$3d^64s(a^4D)4p$] atoms was investigated in He and Ar by laser-induced fluorescence method. The z^3D_J and z^3F_J states of Fe atoms were generated directly by photodissociation of Fe(CO)₅ followed by single photon absorption within a laser pulse using an unfocused laser beam with atomic transition frequencies of Fe. When the z^3D_3 level was excited, the emissions from this level showed a double exponential decay. The fast and slow components of the decay constants from the z^3D_3 level were 10.7×10^{-10} and 0.3×10^{-10} cm³ molecule⁻¹ s⁻¹ in He, and 8.8×10^{-10} and 1.6×10^{-10} cm³ molecule⁻¹ s⁻¹ in Ar, respectively. When the z^3F_4 level was pumped, the emissions from this level showed a single exponential decay and the decay constants were the same as those of the slow components of z^3D_3 . The emissions from higher-lying levels were single exponential at low pressures and the decay constants were in the range of $0.7\text{--}3.6 \times 10^{-10}$ cm³ molecule⁻¹ s⁻¹. It is found that the collisional mixing between the z^3D_3 and z^3F_4 levels is very fast in both buffer gases while the mixing among the higher-lying four levels is relatively slow. The radiative lifetimes of the z^3D_J and z^3F_J levels were 280–370 and 770–1100 ns, respectively, depending on J . Kinetic simulations of time profiles from the laser excited and collisional product levels revealed that intermultiplet mixing appeared to be more efficient than intramultiplet mixing. © 1996 American Institute of Physics. [S0021-9606(96)01241-X]

I. INTRODUCTION

It is well known that the refractive metal atoms in the gas phase can be generated by multiphoton dissociation (MPD) of metal carbonyls or organometallic compounds.^{1–6} However, most of the MPD studies were done using a focused laser beam, and various excited states of metal atoms were found to be generated simultaneously under these experimental conditions.^{1–3} Since the product states are not unique when a focused beam is used for MPD of metal carbonyls or organometallic compounds, it is difficult to study kinetic behavior of a state-selected excited state of metal atoms with a one-color laser system.

Recently, we have reported that a state-selected excited state of Fe atoms can easily be generated by MPD of Fe(CO)₅ using an unfocused weak UV laser pulse whose frequency matches exactly to the corresponding Fe atomic transition line.⁷ The efficiency of Fe* formation depends on the frequency of the atomic transition and pulse energy of the laser. In general, the fluorescence from a state-selected excited state of Fe atoms is easily observed when the corresponding two-photon energies of a specified atomic transition line are about 3000 cm⁻¹ in excess compared to the sum of the five Fe–CO bond energies. The power dependence of the fluorescence intensities revealed that the overall process for the formation of the Fe* atoms is a three-photon process.

In this work, we report the results of kinetic studies on the behaviors of the z^3D_J and z^3F_J states of Fe atoms in He and Ar. These states are chosen for the following reasons; (i) they are easily formed by the MPD of Fe(CO)₅ using $a^5D_J \rightarrow z^3D_J$ and $a_5D_J \rightarrow z^3F_J$ atomic transition frequen-

cies of Fe in the 315–325 nm region at low laser pulse energies and the emissions from $z^3D_J \rightarrow a^3F_J$ and $z^3F_J \rightarrow a^3F_J$ transitions are easy to observe; (ii) the radiative lifetimes of these states are expected to be relatively long due to the small Einstein A coefficients⁸ so that they are good candidates for studying kinetic behaviors; and (iii) both the z^3D and z^3F terms arise from the same electronic configuration [$3d^64s(a^4D)4p$] with similar energies but different orbital angular momentum. It is found that the collisional mixing between the z^3D_3 and z^3F_4 levels is very efficient, and kinetic simulations are needed to determine the collisional mixing rate constants and the radiative lifetimes of these levels. However, the collisional mixing among the other higher-lying four levels are not so fast as the lower two levels and the radiative lifetimes of these levels are determined directly from the Stern–Volmer plots obtained from analyzing low pressure time profiles.

II. EXPERIMENTAL METHODS

A detailed experimental set up has been reported in elsewhere.⁹ Briefly, the MPD/LIF cell was made of a 2l Pyrex bulb and two pairs of 1 in. Pyrex O-ring joints were attached to allow laser beam path and to connect to the gas handling vacuum rack. The ports for the fluorescence detection were made by attaching 1.5 in. Pyrex tubings to the bulb and cutting the arms with a glass saw as close as possible to the bulb. The sample gas [0.5% Fe(CO)₅ in He or Ar] was premixed and stored in a storage bulb in the vacuum rack. The gas mixture was slowly flowed through the cell and the flow rate (~0.5 mmol/min) was controlled by adjusting the

openings of the inlet needle valve and exit Teflon valve. Then, the unfocused UV laser pulses ($1.5\text{--}2.5\text{ mJ/cm}^2$) obtained from the frequency doubling of the dye laser output were passed through the cell. The linewidth of our laser (Quantel YG681-TDL 60 with NBP and DGO) was narrow ($<0.1\text{ cm}^{-1}$) enough to excite the single spin-orbit state selectively. The fluorescence from the excited Fe atoms was detected at 90° from the laser beam direction through a 0.5 m monochromator (Spex 1870C) equipped with a holographic grating (2400 grooves/mm) and a Hamamatsu R928 photomultiplier (PM) tube. It was possible to monitor the near-lying fluorescences from the z^3D_3 and z^3F_4 levels separately by employing $200\text{ }\mu\text{m}$ of the slitwidth. Atomic emission wavelengths from other levels were not so close that $300\text{ }\mu\text{m}$ of the slitwidth was good enough to monitor the emissions from the different spin-orbit levels. The signal from the PM tube was fed into a transient digitizer (Tektronix 7912HB) and transferred to a laboratory computer for signal averaging and storage. Small portions of the dye laser beam was directed to a fast response photodiode and the signal from the photodiode was used to trigger the digitizer. The $\text{Fe}(\text{CO})_5$ was purchased from Aldrich, and transferred to a loading vessel in a glovebox filled with dry N_2 . Then the sample was further purified by freeze and thaw method on the vacuum rack before making a mixture.

III. RESULTS

A. Kinetics between the z^3D_3 and z^3F_4 levels

Schematic energy levels of the relevant states in this work are shown in Fig. 1. When the laser frequency was tuned to the $z^3D_3 \leftarrow a^5D_4$ transition line of the Fe atom and directed to the cell containing a mixture of 0.5% $\text{Fe}(\text{CO})_5$ in He/Ar, the fluorescences from the z^3D_3 and z^3F_4 levels were observed. Typical time profiles for the $z^3D_3 \rightarrow a^3F_4$ and $z^3F_4 \rightarrow a^3F_4$ emissions observed from the $z^3D_3 \leftarrow a^5D_4$ and $z^3F_4 \leftarrow a^5D_4$ excitation at 2.0 Torr of a He mixture are plotted in Fig. 2. Although the difference in the fluorescence wavelengths for the $z^3D_3 \rightarrow a^3F_4$ and $z^3F_4 \rightarrow a^3F_4$ transitions is small, the emissions can be effectively separated by using $200\text{ }\mu\text{m}$ slitwidth of the monochromator. The separation of the fluorescences from these levels was confirmed from the different shapes in the rise times of the time profiles for the laser excited and product levels. When the z^3D_3 level was populated, the fluorescence from the laser excited level was strong and clearly showed a double exponential decay. The emission from the z^3F_4 level was weak and appeared to be a single exponential decay as shown in Fig. 2(a). When the z^3F_4 level was populated, the fluorescence from the laser excited level was weak compared to that from the z^3D_3 level as shown in Fig. 2(b). The same trend was observed in an Ar mixture. Since the energy difference between the z^3D_3 and z^3F_4 levels is about 15 cm^{-1} , collisional mixing between the two levels appears to be very efficient. Also, the strong emissions from the z^3D_3 level when the z^3F_4 level was excited suggest that the radiative lifetime of the z^3D_3 level is much shorter than that of the z^3F_4 level.

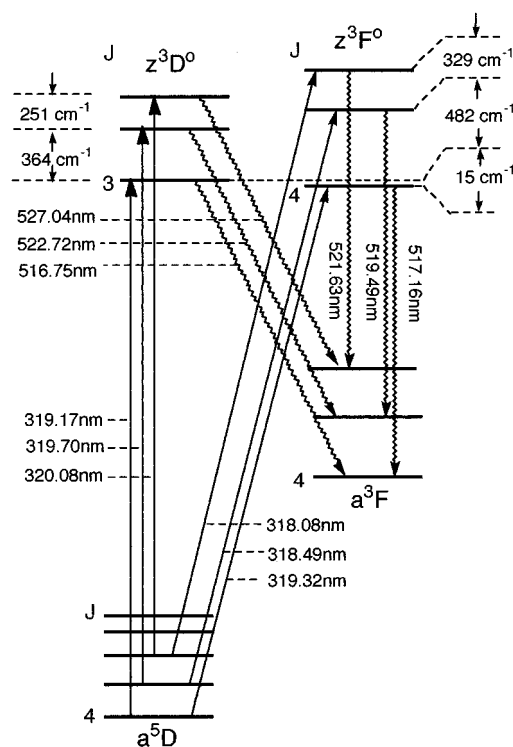


FIG. 1. Schematic energy level diagram for $\text{Fe}(a^5D_J, a^3F_J, z^3F_J, \text{ and } z^3D_J)$.

The decay curves for the $z^3D_3 \rightarrow a^3F_4$ emission from the $z^3D_3 \leftarrow a^5D_4$ excitation in He and Ar were analyzed by a double exponential fitting. The pressure dependence of the decay rates of the fast component is plotted in Fig. 3(a) and that of the slow component is shown in Fig. 3(b). Also shown in Fig. 3(b) is the pressure dependence of the decay rates for the $z^3F_4 \rightarrow a^3F_4$ emission from the $z^3F_4 \leftarrow a^5D_4$ excitation analyzed by a single exponential fitting. It is interesting that the pressure dependence of the decay rates of the z^3F_4 level is virtually the same as that of the slow component of the laser excited z^3D_3 level in both buffer gases. Furthermore, the zero pressure intercepts for the fast and slow components are the same within the experimental errors. All the rate constants and the zero pressure intercepts are shown in Table I.

We have attempted to find out the physical meaning of the experimental rate constants as well as the zero pressure intercepts by fitting this system to the well-known three-level kinetic scheme,¹⁰ which is described by the following Eq. (1):

$$\begin{aligned}
 A = z^3D_3 &\xrightleftharpoons[k_{-2}]{k_2} z^3F_4 = B \\
 K_1 \downarrow & \qquad \qquad \downarrow K_3 \\
 & a^3F_4 \\
 K_1 = 1/\tau_A + k^{QA}[M], & \qquad \qquad \qquad (1)
 \end{aligned}$$

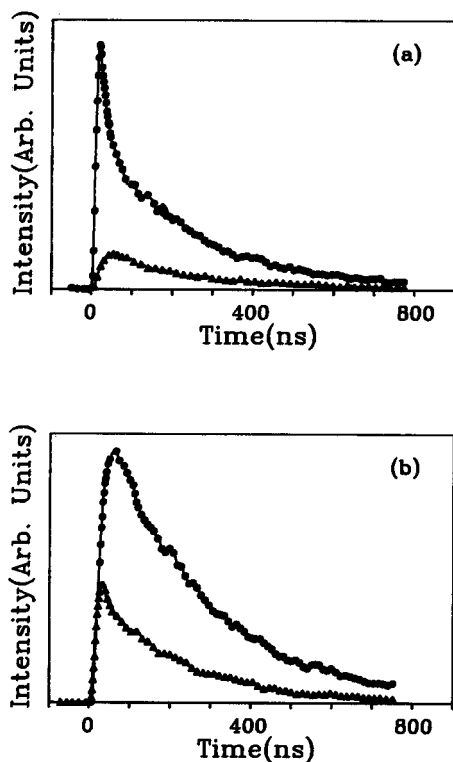


FIG. 2. Typical time profiles obtained from 2.0 Torr of 0.5% Fe(CO)₅ in He: (a) emissions from the z^3D_3 (●-●) and z^3F_4 (▲-▲) levels when the z^3D_3 level was excited, and (b) those from the z^3D_3 (●-●) and z^3F_4 (▲-▲) levels when the z^3F_4 level was laser excited. Only one from five data points are plotted for the decay part of the time profile.

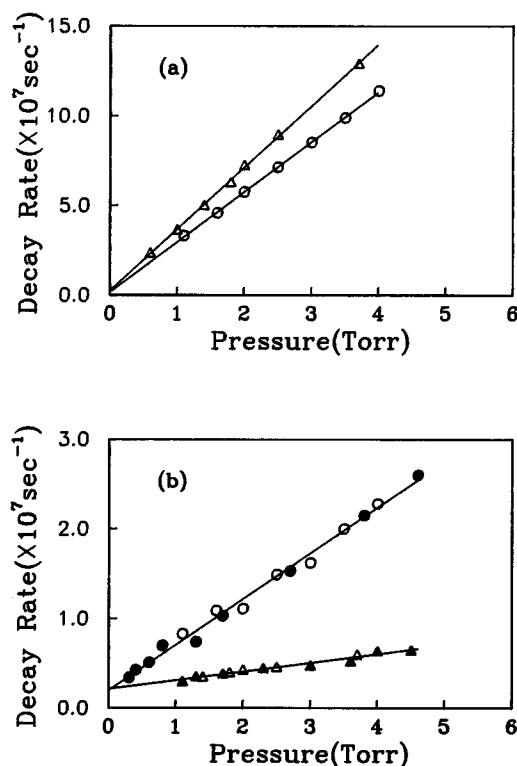


FIG. 3. The pressure dependence of the the decay constants in He (△-△) and in Ar (○-○) for (a) the fast and (b) the slow components when the z^3D_3 level was excited. Also shown in (b) are the pressure dependence of the single exponential decay constants of the z^3F_4 emissions in Ar (●-●) and in He (▲-▲) when the z^3F_4 level was excited.

$$K_2 = k^{AB}[M],$$

$$K_{-2} = k^{BA}[M],$$

$$K_3 = 1/\tau_B + k^{QB}[M],$$

$$\tau_A = \text{radiative lifetime for the } z^3D_3,$$

$$\tau_B = \text{radiative lifetime for the } z^3F_4,$$

$$k^{QA} = \text{quenching rate constant for the } z^3D_3 \text{ by } M,$$

$$k^{QB} = \text{quenching rate constant for the } z^3F_4 \text{ by } M,$$

$$k^{AB} = \text{mixing rate constant from the } z^3D_3$$

to the z^3F_4 ,

$$k^{BA} = \text{mixing rate constant from the } z^3F_4$$

to the z^3D_3 ,

$$M = \text{buffer gas.}$$

The coupled differential equations for the above scheme can be written as Eq. (2),

$$\frac{d[A]}{dt} = -(K_1 + K_2)[A] + K_{-2}[B],$$

$$\frac{d[B]}{dt} = K_2[A] - (K_{-2} + K_3)[B]. \quad (2)$$

The standard solution to the coupled equations is

$$[A(t)] = [A(0)](\lambda_+ - \lambda_-)^{-1} [(\lambda_- + K_1 + K_2)e^{-\lambda_+ t} + (\lambda_+ - K_1 - K_2)e^{-\lambda_- t}],$$

$$[B(t)] = [A(0)]K_2(\lambda_+ - \lambda_-)^{-1} [e^{-\lambda_- t} - e^{-\lambda_+ t}], \quad (3)$$

where the two decay constants are given by Eq. (4),

$$\lambda_{\pm} = \frac{1}{2} \{ (K_1 + K_2 + K_{-2} + K_3) \pm [(K_1 + K_2 - K_{-2} - K_3)^2 + 4K_2K_{-2}]^{1/2} \}. \quad (4)$$

The square root term in Eq. (4) can be rewritten as Eq. (5),

$$\begin{aligned} & [(K_1 + K_2 - K_{-2} - K_3)^2 + 4K_2K_{-2}]^{1/2} \\ &= [(K_2 + K_{-2})^2 + (K_1 - K_3)^2 \\ &+ 2(K_1 - K_3)(K_2 - K_{-2})]^{1/2}. \end{aligned} \quad (5)$$

If $(K_2 + K_{-2})^2 \gg (K_1 - K_3)^2 + 2(K_1 - K_3)(K_2 - K_{-2})$, the second term of Eq. (4) can be approximated as Eq. (6),

$$[(K_1 + K_2 - K_{-2} - K_3)^2 + 4K_2K_{-2}]^{1/2} \approx K_2 + K_{-2}. \quad (6)$$

Then, the decay constants can be reduced to Eq. (7),

TABLE I. Measured rate constants from the Stern–Volmer analysis for z^3D_J and z^3F_J levels of Fe.

Buffer gas	Laser excited level	Quenching rate constants ^a	Intercepts ($\times 10^6$ s ⁻¹)	Radiative lifetimes (ns)	
He	z^3D_3	10.7 ± 0.3	2.0 ± 0.5	$(370 \pm 20)^b$	fast comp. slow comp. coupled decay
		0.30 ± 0.05	2.0 ± 0.2		
	z^3F_4	0.30 ± 0.05	2.0 ± 0.2	$(770 \pm 100)^b$	
	z^3D_2	2.3 ± 0.2	2.7 ± 0.3	370 ± 40	
	z^3D_1	3.0 ± 0.3	3.6 ± 0.3	280 ± 30	
	z^3F_3	3.6 ± 0.3	1.4 ± 0.4	700 ± 200	
z^3F_2	2.0 ± 0.3	0.9 ± 0.2	1100 ± 200		
Ar	z^3D_3	8.8 ± 0.3	2.2 ± 0.6	$(370 \pm 20)^b$	fast comp. slow comp. coupled decay
		1.6 ± 0.4	1.9 ± 0.3		
	z^3F_4	1.6 ± 0.4	2.0 ± 0.3	$(770 \pm 100)^b$	
	z^3D_2	1.2 ± 0.2	3.1 ± 0.3	320 ± 40	
	z^3D_1	1.8 ± 0.2	3.6 ± 0.2	280 ± 30	
	z^3F_3	2.3 ± 0.5	1.1 ± 0.3	900 ± 200	
z^3F_2	0.7 ± 0.2	0.9 ± 0.2	1100 ± 200		

^aUnits, 10^{-10} cm³ molecule⁻¹ s⁻¹.^bAssigned from kinetic simulations of time profiles.

$$\lambda_+ \cong (K_2 + K_{-2}) + \frac{1}{2} (K_1 + K_3)$$

$$= \left[(k^{AB} + k^{BA}) + \frac{1}{2} (k^{QA} + k^{QB}) \right] [M] + \frac{1}{2} \left(\frac{1}{\tau_A} + \frac{1}{\tau_B} \right),$$

$$\lambda_- \cong \frac{1}{2} (K_1 + K_3) = \frac{1}{2} (k^{QA} + k^{QB}) [M]$$

$$+ \frac{1}{2} \left(\frac{1}{\tau_A} + \frac{1}{\tau_B} \right). \quad (7)$$

Now the physical meanings of the slopes and intercepts obtained from Fig. 3 can be interpreted from Eq. (7). It is clear that the zero pressure intercepts for the fast and slow components should be the same and they are the average value of the lifetimes of the coupled levels. Also, the slope for the fast component of the z^3D_3 level corresponds to the sum of the forward and backward mixing rate constants plus the average value of the purely quenching rate constants of the two levels. The latter is also obtained from the slope of the slow component. It is evident that kinetic simulations of the time profiles are needed to determine the radiative lifetimes of the z^3D_3 and z^3F_4 levels and collisional mixing rate constants, because they cannot be determined directly from the Stern–Volmer analysis. Since the experimental rate constants from the Stern–Volmer analysis and the equilibrium constant expression given by Eq. (8), provide good boundary conditions, it was possible to extract the radiative lifetimes of these levels and mixing rate constants by kinetic simulations of the time profiles,

$$K_{\text{eq}} = k^{BA}/k^{AB}$$

$$= (g^A/g^B) \exp(-\Delta E/kT) = 0.724 \text{ at } 300 \text{ K}. \quad (8)$$

To fit the shapes and relative intensities of time profiles from both z^3D_3 and z^3F_4 levels, the following sets of rate constants were assigned in He and Ar, respectively

$$k^{AB} = 6.1 \times 10^{-9}(\text{He}); 4.0 \times 10^{-9}(\text{Ar}) \text{ cm}^3 \text{ molecule}^{-1} \text{ s}^{-1},$$

$$k^{BA} = 4.5 \times 10^{-9}(\text{He}); 2.8 \times 10^{-9}(\text{Ar}) \text{ cm}^3 \text{ molecule}^{-1} \text{ s}^{-1},$$

$$k^{QA} = k^{QB} = 0.3 \times 10^{-10}(\text{He});$$

$$1.6 \times 10^{-10}(\text{Ar}) \text{ cm}^3 \text{ molecule}^{-1} \text{ s}^{-1},$$

$$\tau_A = 370 \pm 20 \text{ ns},$$

$$\tau_B = 770 \pm 100 \text{ ns}. \quad (9)$$

Figure 4 shows the comparison of the experimental and cal-

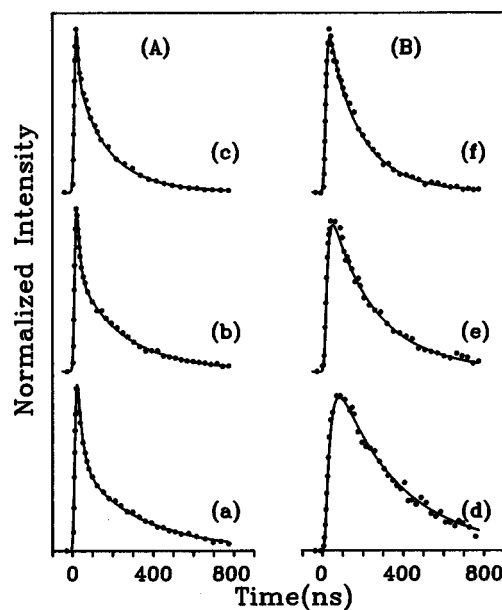


FIG. 4. Comparison of the experimental (\cdots) and simulated ($—$) time profiles for (a) $z^3D_3 \rightarrow a^3F_4$ and (b) $z^3F_4 \rightarrow a^3F_4$ emissions at three different pressures when the z^3D_3 level was excited. (a), (d) 1.0 Torr; (b), (e) 2.0 Torr; and (c), (f) 4.0 Torr of 0.5% Fe(CO)₅ in He. Only one from five data points were plotted for the decay part of the experimental time profiles.

culated time profiles at three different pressures using the above rate constants. Because of the small energy difference between the z^3D_3 and z^3F_4 levels, the quenching rate constants for both levels were assumed to be the same. Note that the radiative lifetime of the z^3D_3 level has to be assigned much shorter than that of the z^3F_4 level to fit the relative emission intensities of the time profiles shown in Fig. 2. It is interesting that the collisional mixing between these two levels is more efficient in He than in Ar. While less than 10% of the experimentally measured apparent quenching rate constants are assigned to other states in He, about 30%–40% of the apparent quenching rate constants are assigned to other states in Ar to fit the shapes of experimental time profiles.

B. Kinetics of the higher-lying $z^3D_{2,1}$ and $z^3F_{3,2}$ levels

1. Radiative lifetimes and apparent quenching rate constants

The higher-lying four levels were excited at 319.70($z^3D_2 \leftarrow a^5D_3$), 320.08($z^3D_1 \leftarrow a^5D_2$), 318.49($z^3F_3 \leftarrow a^5D_3$), and 318.08 nm($z^3F_2 \leftarrow a^5D_2$), and the emissions were monitored at 522.72($z^3D_2 \rightarrow a^3F_3$), 527.04($z^3D_1 \rightarrow a^3F_2$), 519.49($z^3F_3 \rightarrow a^3F_3$), and 521.63 nm($z^3F_2 \rightarrow a^3F_2$), respectively, as shown in Fig. 1. The excitation wavelengths in the 318–320 nm region were chosen for convenience since the fluorescence from the $z^3D_{2,1}$ and $z^3D_{3,2}$ were strong enough to investigate kinetic behavior when these levels were generated from the $a^5D_{3,2}$ levels. The time profiles from these higher-lying levels showed apparent single exponential decay at low pressures but they revealed double or even triple exponential decay behavior at higher pressures. Since the reliable analysis of the time profiles obtained at higher pressures was difficult, we concentrated our efforts to obtain good time profiles at low pressures (<2 Torr) and analyzed them by a single exponential fitting. The pressure dependence of the decay constants below 2 Torr of total pressures is plotted in Fig. 5. The fluorescence from the z^3F_3 and z^3F_2 levels was very weak at low pressures, and a large number of signal averaging were needed to obtain analyzable time profiles.

The apparent quenching rate constants as well as the radiative lifetimes for these levels are shown in Table I. The magnitudes of the apparent quenching rate constants are substantially larger in He($2.0\text{--}3.6 \times 10^{-10}$ cm³ molecule⁻¹ s⁻¹) than in Ar($0.7\text{--}1.8 \times 10^{-10}$ cm³ molecule⁻¹ s⁻¹). The quenching rate constants for the z^3F_3 and z^3D_1 levels are substantially larger than those for the z^3F_2 and z^3D_2 levels in both buffer gases probably due to the near-lying energy levels. The radiative lifetimes obtained from the two buffer gases agree well within the experimental errors, however, the radiative lifetimes from the Ar buffer gas appear to be more reliable than those from the He medium due to the small quenching rate constants.

2. Identification of collisional primary product levels

The apparent quenching rate constants for these levels are not as large as those for the lower-lying z^3D_3 and z^3F_4 levels. However, they are still quite large, $0.7\text{--}3.6 \times 10^{-10}$

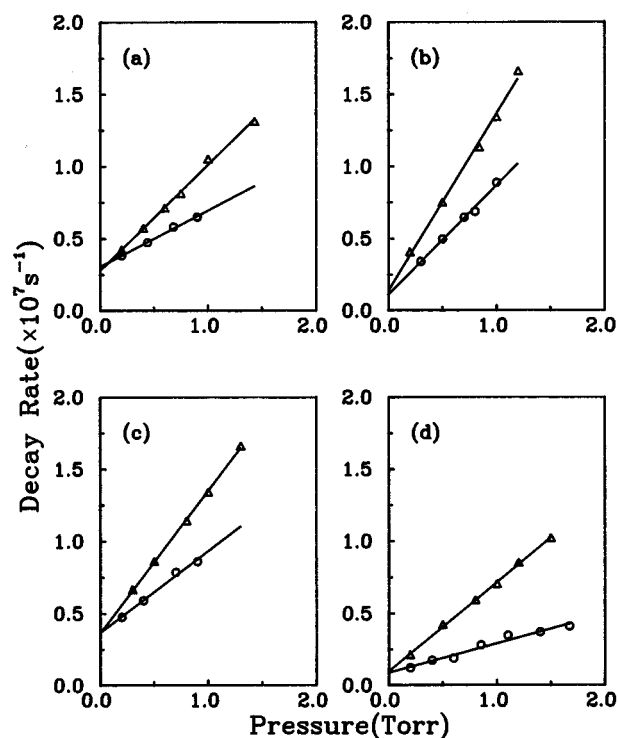


FIG. 5. The pressure dependence of the decay constants in He(Δ - Δ) and in Ar(\circ - \circ) for (a) z^3D_2 , (b) z^3F_3 , (c) z^3D_1 , and (d) z^3F_2 levels.

cm³ molecule⁻¹ s⁻¹, and collisional mixing among these levels is expected. Indeed, collisional mixing among these levels is identified by taking time-resolved fluorescence spectra. Because of the relatively long radiative lifetimes of these levels, the time-resolved fluorescence spectra were taken at low pressures to get information on the primary collisional product levels. A typical time-resolved fluorescence spectra obtained from the z^3F_3 excitation at 1.0 Torr of 0.5% Fe(CO)₅ in Ar are shown in Fig. 6. During the 0–16 ns time period, only the $z^3F_3 \rightarrow a^3F_3$ emission peak appears at 519.5 nm, but emissions from other levels appear at later time periods. Since the radiative lifetimes of the z^3D_J levels are much shorter than that of the initially excited z^3F_3 level, the emissions from the z^3D_J levels are ascribed to the consequence of the collisional mixing among these levels. Also, all the z^3D_J levels appear to be primary collisional products with different branching fractions when the z^3F_3 level was excited.

3. Time profiles from the laser excited and product levels

Since the emissions from the collisional product levels were observed, we attempted to find out the magnitude of intra- and intermultiplet mixing rate constants as well as the collisional branching fractions. For this purpose, we have collected fluorescence time profiles from the laser excited and collisional product levels by pumping each of the spin-orbit levels at low pressures. Typical time profiles from the laser excited and product levels in He and Ar are plotted in

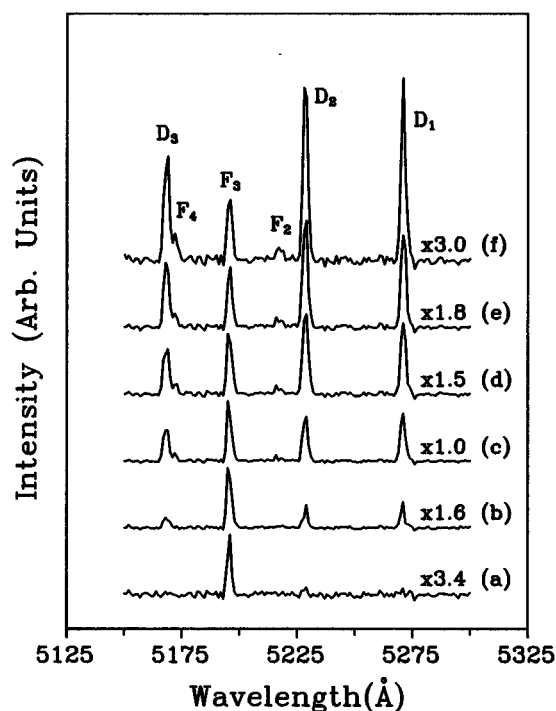


FIG. 6. Time resolved fluorescence spectra from z^3F_3 excitations; (a) 0–16 (b) 16–32, (c) 32–62, (d) 62–92, (e) 92–122, and (f) 122–152 ns periods.

Figs. 7 and 8, respectively, which were obtained at 2.0 Torr of total pressure. The kinetic behaviors observed from each level excitation are described below.

a. Kinetics of z^3D_2 : The z^3D_2 level locates 118 cm^{-1} below the z^3F_3 level and fast mixing between these two levels is expected. When the z^3D_2 level was excited in He and Ar, emissions from the z^3D_3 , z^3D_1 , and z^3F_3 levels were observed as shown in Figs. 7(a) and 8(a), respectively. Note that the emission from the z^3D_3 located 364 cm^{-1} below the laser excited level was much stronger than that from z^3F_3 and z^3D_1 levels. The shape and relative intensity of the time profile from the z^3D_3 level in He are much different from those in Ar although the rise times are similar. About four times stronger peak intensity and much slower decay of the z^3D_3 emission in He is consistent with the strong coupling between the z^3D_3 and z^3F_4 levels as described in Sec. III A. Much faster decay and weaker intensity of the z^3D_3 emission in Ar is ascribed to the weaker coupling between the z^3D_3 and z^3F_4 levels and larger quenching rate constants by Ar. The weak emission intensities from the z^3F_3 level might be due to the much smaller Einstein A coefficient for the $z^3F_3 \rightarrow a^3F_3$ transition ($A_{ik} = 2.9 \times 10^5\text{ s}^{-1}$) than for $z^3D_{3,2} \rightarrow a^3F_{3,2}$ transition ($A_{ik} = 2.0\text{--}2.5 \times 10^6\text{ s}^{-1}$) at the observed wavelength.⁸

b. Kinetics of z^3F_3 : The z^3F_3 level locates 118 cm^{-1} above the z^3D_2 and 133 cm^{-1} below the z^3D_1 level. Since the energy differences from these near-lying levels are small, fast collisional mixing among them is expected. When the z^3F_3 level was excited at 2.0 Torr of total pressure in He, collisional product emissions from $z^3D_{1,2,3}$ levels were even stronger than the directly pumped level as plotted in Fig.

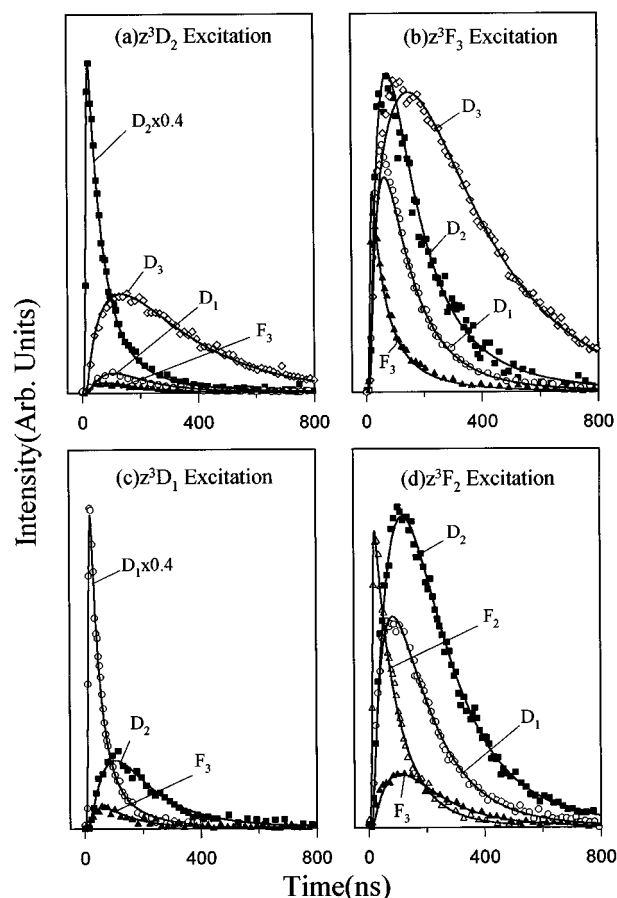


FIG. 7. Comparison of experimental z^3D_2 (■—■), z^3D_3 (◇—◇), z^3D_1 (○—○), z^3F_3 (▲—▲), z^3F_2 (△—△), and calculated (—) time profiles in He. The experimental time profiles are plotted one from every five data points to avoid congestion. The emission intensities of the laser excited z^3D_2 and z^3D_1 levels in (a) and (c) were reduced to 40% of their experimental intensities.

7(b). The rise time of these product emissions is more or less the same, but the peak intensities are in the order of $z^3D_2 \cong z^3D_3 > z^3D_1$. Also, the emission from the z^3D_3 decays slowly compared to those from other levels. The slower decay of the z^3D_3 emission might be ascribed to the tight coupling with the z^3F_4 level in He. When the z^3F_3 level was excited in Ar using the same laser power, the relative emission intensities are in the order of $z^3D_2 > z^3D_1 \cong z^3D_3$ as shown in Fig. 8(b).

c. Kinetics of z^3D_1 : The z^3D_1 level locates 133 and 251 cm^{-1} above the z^3F_3 and z^3D_2 , respectively, and 196 cm^{-1} below the z^3F_2 . When this level was populated in He and Ar, collisional product emissions from the z^3D_2 and z^3F_3 levels were easily observed, but the emission from the z^3F_2 level was very weak and not plotted. The emission from the z^3D_2 level was much stronger than that from the z^3F_3 as shown in Figs. 7(c) and 8(c). The rise and decay of the z^3D_2 emission appeared to be somewhat than those of the z^3F_3 in both buffer gases. The delayed appearance of the z^3D_2 emission suggests that this level might be affected by secondary collisional processes.

d. Kinetics of z^3F_2 : The z^3F_2 level locates 196 and 329

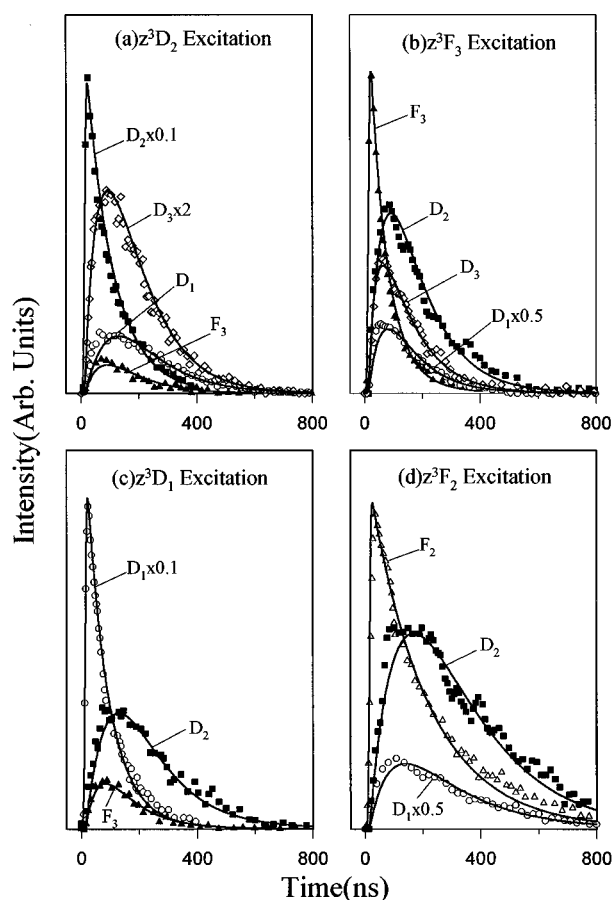


FIG. 8. Comparison of experimental z^3D_2 (■-■), z^3D_3 (◇-◇), z^3D_1 (○-○), z^3F_3 (▲-▲), z^3F_2 (△-△), and calculated (—) time profiles in Ar. The experimental time profiles are plotted one from every five data points to avoid congestions. The emission intensities of the laser excited z^3D_2 and z^3D_1 levels in (a) and (c) were reduced to 10% of their experimental intensities. The intensity of the z^3D_3 emission was magnified by a factor of 2 to avoid congestion.

cm^{-1} above the z^3D_1 and z^3F_3 levels, respectively. When this level was excited in He and Ar, emissions from the z^3D_1 , z^3F_3 , and z^3D_2 levels were observed. The emission from z^3D_2 level lying 463 cm^{-1} below was stronger than other emissions but appeared with time delay as shown in Figs. 7(d) and 8(d). The emission from the z^3D_2 level might also be affected by secondary collisional processes as for the z^3D_1 excitation.

4. Kinetic simulations and assignment of collisional branching fractions

Although the collisional energy transfer processes among the $z^3D_{2,1}$ and $z^3F_{3,2}$ levels in He and Ar seemed to be very complicated, those kinetic behaviors of each level described above provided some clue for assigning collisional branching fractions among these levels by kinetic simulations of the time profiles. When one of these levels was populated by a laser pulse, emissions from all the near-lying levels appeared. Also, preliminary calculations showed that those time profiles from the collisional product levels could not fit satisfactorily using two-level coupling scheme.¹⁰

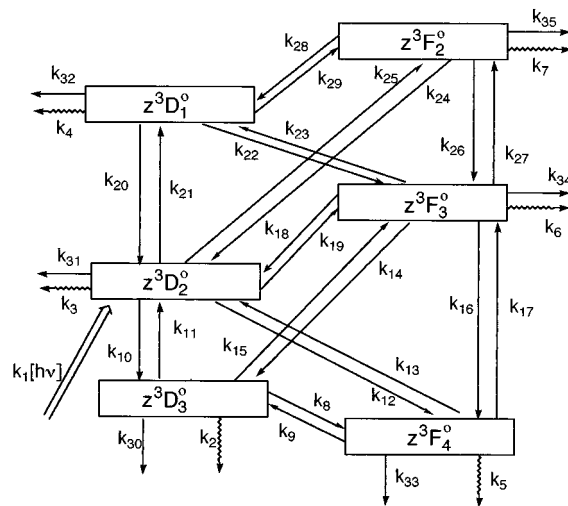


FIG. 9. Kinetic scheme for the calculations of time profiles. (k_1 , arbitrary absorption rate constant; k_2 – k_7 , radiative rate constants; k_8 – k_{29} , inter- and intramultiplet mixing rate constants; and k_{30} – k_{35} , quenching rate constants to other states.)

Thus, we set up more complicated kinetic scheme shown in Fig. 9, which includes 6 species and 35 rate constants. When the initially excited level, primary and secondary collisional product levels are denoted as i , n , and m , respectively, the time dependence of the initially excited and primary level populations can be written as Eq. (9),

$$d[N_i]/dt = F(t) - [N_i] \left\{ 1/\tau_i + \left(\sum_n k_{in} + k_i^q \right) [M] \right\} + \sum_n k_{ni} [M] [N_n] + \sum_m k_{mi} [M] [N_m], \quad (9a)$$

$$d[N_n]/dt = k_{in} [N_i] [M] - [N_n] \left\{ 1/\tau_n + \left(k_{ni} + \sum_m k_{nm} + k_n^q \right) \times [M] \right\} + \sum_m k_{mn} [M] [N_m] + \sum_{n'} k_{n'n} [M] [N_{n'}]. \quad (9b)$$

The $F(t)$ is the formation rate of the species by the laser pulse, τ is the radiative lifetime, k_{jp} represents collisional mixing rate constant from j to p level belonging to the z^3D and z^3F term, k^q is the quenching rate constant to other states and subscript n' denotes other near-lying primary levels. Since the intensities of the experimentally observed time profiles depend on the magnitude of Einstein A coefficient at the observed wavelength, and since the Einstein A coefficient for each level at the observed wavelength shows large differences, conversion of $I(t)$ to $N(t)$ was needed to compare not only the shapes but also the relative intensities of the experimental and calculated time profiles. Thus, those experimentally obtained time profiles $[I(t)]$ were divided by the Einstein coefficients A_{ik} to convert populations, where A_{ik} is the Einstein A coefficient for the observed line.⁸ The assignment of state-to-state collisional mixing/quenching rate constants was based on the apparent total quenching rate

TABLE II. Rate constants used for kinetic simulation and branching fractions (Γ) for z^3D_J and z^3F_J levels of Fe in He and in Ar.

Process	Rate constants ^a	Γ	ΔE^b (cm ⁻¹)	$ \Delta L $	$ \Delta J $	σ^c (Å ²)
$z^3D_3 + \text{He} \rightarrow z^3F_4$	61	0.93	15	1	1	46.9
$\rightarrow z^3D_2$	0.8	0.01	-364	0	1	0.6
$\rightarrow z^3F_3$	0.6	<0.01	-482	1	0	0.5
\rightarrow others	3.3	0.05				2.5
$z^3D^2 + \text{He} \rightarrow z^3F_3$	9.0	0.36	-118	1	1	6.9
$\rightarrow z^3D_3, z^3F_4$	13.0	0.52	364,379	0,1	1,2	10.0
$\rightarrow z^3D_1$	0.8	0.03	-251	0	1	0.6
$\rightarrow z^3F_2$	0.6	0.02	-447	1	0	0.5
\rightarrow others	1.5	0.06				1.2
$z^3D_1 + \text{He} \rightarrow z^3F_3$	24	0.70	133	1	2	18.5
$\rightarrow z^3F_2$	4.0	0.12	-196	1	1	3.1
$\rightarrow z^3D_2$	4.0	0.12	251	0	1	3.1
\rightarrow others	2.0	0.06				1.5
$z^3F_4 + \text{He} \rightarrow z^3D_3$	45	0.91	-15	1	1	34.6
$\rightarrow z^3D_2$	0.6	0.01	-379	1	2	0.5
$\rightarrow z^3F_3$	0.4	<0.01	-497	0	1	0.3
\rightarrow others	3.3	0.07				2.5
$z^3F_3 + \text{He} \rightarrow z^3D_2$	12	0.39	118	1	1	9.2
$\rightarrow z^3D_1$	6.0	0.19	-133	1	2	4.6
$\rightarrow z^3D_3, z^3F_4$	11	0.36	482,497	1,0	0,1	8.5
\rightarrow others	1.0	0.03				0.8
$z^3F_2 + \text{He} \rightarrow z^3D_1$	8.0	0.42	196	1	1	6.2
$\rightarrow z^3F_3$	7.0	0.37	329	0	1	5.4
$\rightarrow z^3D_2$	5.5	0.29	447	1	0	4.2
\rightarrow others	0.5	0.02				0.4
$z^3D_3 + \text{Ar} \rightarrow z^3F_4$	40	0.68	15	1	1	76.9
$\rightarrow z^3D_2$	0.3	<0.01	-364	0	1	0.6
z^3F_3	0.2	<0.01	-482	1	0	0.4
\rightarrow others	18	0.31				34.6
$z^3D_2 + \text{Ar} \rightarrow z^3F_3$	3.3	0.26	-118	1	1	6.3
$\rightarrow z^3D_3, z^3F_4$	4.0	0.32	364,379	0,1	1,2	7.7
$\rightarrow z^3D_1$	0.4	0.03	-251	0	1	0.8
$\rightarrow z^3F_2$	0.2	0.02	-447	1	0	0.4
\rightarrow others	4.7	0.37				9.0
$z^3D_1 + \text{Ar} \rightarrow z^3F_3$	8.5	0.54	133	1	2	16.3
$\rightarrow z^3F_2$	1.5	0.10	-196	1	1	2.9
$\rightarrow z^3D_2$	1.8	0.11	251	0	1	3.5
\rightarrow others	3.9	0.25				7.5
$z^3F_4 + \text{Ar} \rightarrow z^3D_3$	28	0.60	-15	1	1	53.8
$\rightarrow z^3D_2$	0.2	<0.01	-379	1	2	0.4
$\rightarrow z^3F_3$	0.2	<0.01	-497	0	1	0.4
\rightarrow others	18	0.39				34.6
$z^3F_3 + \text{Ar} \rightarrow z^3D_2$	4.0	0.16	118	1	1	7.7
$\rightarrow z^3D_1$	2.3	0.09	-133	1	2	4.4
$\rightarrow z^3D_3, z^3F_4$	6.0	0.24	482,497	1,0	0,1	11.5
\rightarrow others	12	0.50				23.0
$z^3F_2 + \text{Ar} \rightarrow z^3D_1$	1.8	0.28	196	1	1	3.5
$\rightarrow z^3F_3$	1.2	0.18	329	0	1	2.3
$\rightarrow z^3D_2$	1.8	0.28	447	1	0	3.5
\rightarrow others	1.7	0.26				3.3

^aUnits, 10⁻¹¹ cm³ molecule⁻¹ s⁻¹.

^b $\Delta E = E(\text{initial level}) - E(\text{product level})$.

^c $\sigma = k/\langle v \rangle$; $\langle v \rangle = (8kT/\pi\mu)^{1/2} = 1300$ m/s (in He) and 520 m/s (in Ar) at 298 K.

constant shown in Table I, and adjusted to match the shapes and relative intensities of the time profiles from the laser excited and collisional product levels. The solid lines in Figs. 7 and 8 are the calculated time profiles at 2.0 Torr of total pressure, and state-to-state rate constants are given in Table II. In fact, the state-to-state rate constants shown in Table II were obtained from such a comparison of experimental and

simulated time profiles at various pressures. The branching fraction Γ and cross section σ are calculated from the simple relation,

$$\Gamma_{i,j} = k_{ij} / \sum k_{ij} = k_{ij} / k^{\text{total}}, \quad (10)$$

$$\sigma_{ij} = k_{ij} / \langle v \rangle = k_{ij} / (8kT/\pi\mu)^{1/2}, \quad (11)$$

where k^Q is the apparent total quenching rate constant for the laser excited level, and μ is the reduced mass.

In general, experimentally observed emission intensities from the $z^3F_{3,2}$ levels were much weaker than those from the $z^3D_{1,2,3}$ due to the small Einstein A coefficients at the observed wavelengths. Since the Fuhr and co-workers' Einstein A coefficients⁶ were used to correct emission intensities of the time profiles, and since the branching fractions in Table II were obtained from the shapes and the time integrated emission intensities of the time profiles, some difference in the Einstein A coefficients of the $z^3F_{3,2}$ levels may propagate substantial difference in the branching fractions. However, the branching fractions in Table II clearly show the following features for the collisional mixing among the z^3D_J and z^3F_J levels: (i) Collisional mixing among the z^3D_J and z^3F_J levels is much more extensive in He than in Ar, although the absolute quenching cross sections for the laser excited level appear to be opposite. Collisional branching fractions to other states are less than 10% in He, but they become 25%–50% in Ar. (ii) Energy loss ($\Delta E > 0$) collisions are more efficient than energy gain ($\Delta E < 0$) collisions in both buffer gases. When the z^3D_2 level was excited, formation of the z^3D_3 and z^3F_4 levels lying 364 and 379 cm^{-1} below, respectively, appeared to be more favorable than that of z^3F_3 level lying 118 cm^{-1} above. When the z^3F_3 level was excited, formation of z^3D_3 and z^3F_4 levels ($\Delta E \approx 490 \text{ cm}^{-1}$) also seemed to be more efficient than that of z^3D_1 lying 139 cm^{-1} above. (iii) Intermultiplet mixing ($\Delta L = \pm 1$) appears to be more efficient in both buffer gases due to the smaller energy differences, although the observed product emissions from the z^3D_J were much stronger than those from the z^3F_J .

IV. DISCUSSION

The kinetics between the z^3D_3 and z^3F_4 levels are very interesting. The energy difference between the two levels is only 15 cm^{-1} and fast collisional mixing between them is expected. Because of the large collisional mixing rate constants between the two levels and the relatively long radiative lifetimes as well as the small average quenching rate constants of the two levels, the experimental rate constant for the fast component of the z^3D_3 level is dominated by the sum of the mixing rate constants between the two levels. Similar kinetics were observed for the collisional coupling and relaxation study of $\text{N}_2(B)$ and $\text{N}_2(W)$ vibrational levels¹¹ and the vibrational relaxation study of the a^3B_1 state of SO_2 .¹²

It is also interesting that the radiative lifetimes of the intramultiplet levels of the z^3D term have a tendency of getting shorter as the energy is higher, and those of the z^3F term show an opposite trend. A significantly different radiative lifetimes of intramultiplet levels have also been reported for the z^3P term of an Fe atom by Figger *et al.*¹³ Marek and co-workers¹⁴ reinvestigated the radiative lifetimes of the z^3P_J and obtained 108, 94, and 37 ns for $J=0, 1,$ and $2,$ respectively. They attributed their observations on the z^3P_J levels to the inappropriate LS-coupling scheme for the z^3P state. The $z^3F, z^3D,$ and z^3P states arise from the same

electron configuration, $3d^64s(a^4D)4p$, so that the different radiative lifetimes of the spin-orbit levels belonging to the same term could be attributed to the same reason.

It was found that the experimentally measured radiative lifetimes of the z^3D_J and z^3F_J levels were shorter than the radiative lifetimes calculated from the sum of Einstein A coefficients tabulated in Ref. 8. To investigate these discrepancies, we scanned the monochromator to look for any missing radiative transitions from the laser excited level. It was very difficult to find out missing transitions for the z^3F_J levels due to the small Einstein A coefficients as well as the fast collisional transfer to the near-lying z^3D_J levels, however, we were able to identify some of the missing transitions from the z^3D_J levels. For instance, the $z^3D_2 \rightarrow a^3F_3$ transition at 522.7 nm gave the strongest fluorescence from the z^3D_2 excitation but was missing in Ref. 8. When the emission intensity at 522.7 nm was converted to the Einstein A coefficient comparing with those of other tabulated transitions, the sum of A coefficients for the z^3D_2 level gave good agreement with the experimental value. Thus, the individual A coefficient tabulated in Ref. 8 seemed to be reliable even though the table does not include every plausible transitions. Since the branching fractions shown in Table II were obtained from the kinetic simulations of time profiles, and since the Einstein A coefficients in Ref. 8 were used to correct emission intensities of the time profiles at the observed wavelengths, the reliability of the branching fractions in Table II should not be so bad.

The apparent quenching rate constants for the z^3D_J and z^3F_J levels of the Fe atom by He and Ar in this work are much larger than those previously reported values for the low-lying excited states of group 1, 2, and 12 metal atoms tabulated by Breckenridge and Umemoto.¹⁵ One of the reasons for those small quenching cross sections tabulated in Ref. 15 is that they do not include intramultiplet mixing processes. In fact, large intramultiplet mixing cross sections in collision with rare gases have been reported for the low-lying excited state of $\text{Li}(2^2P_J), \text{Na}(3^2P_J), \text{K}(4^2P_J \text{ and } 5^2P_J), \text{Rb}(9^2D_J),$ and $\text{Ca}(4s5p^3P_J),$ where the energy gap between the intramultiplet levels is small ($\Delta E < 60 \text{ cm}^{-1}$).^{16–22} It has also been reported that the intramultiplet mixing cross sections are small for low-lying excited states of Sr, Zn, Cd, and Hg where the energy gap between the intramultiplet levels is large ($\Delta E > 180 \text{ cm}^{-1}$).^{23–29} Parson and Ishikawa³⁰ also studied intramultiplet mixing collisions of $\text{Cr}(3d^54p \ z^7P_J)$ with various gases. The intramultiplet splitting of $\text{Cr}(3d^54p \ z^7P_J)$ are 81.3 and 112.5 cm^{-1} , respectively. They obtained 11–18 \AA^2 for the intramultiplet mixing cross sections by He and Ar at the effective temperature of 405 and 951 K, respectively. The results of these collisional intramultiplet mixing studies reveal that the apparent collisional quenching rate constants depend upon the existence of near-lying energy states and the shapes of interaction potentials. Although the intramultiplet splitting energies for the z^3D_J and z^3F_J levels of Fe atoms are not small as shown in Fig. 1, the relatively small energy differences between the nearest intermultiplet levels seemed to provide complicated $\text{Fe}^*-\text{He}/\text{Ar}$ interaction po-

tentials leading to large collisional quenching of the z^3D_J and z^3F_J levels.

V. CONCLUSION

We have studied collisional mixing among the z^3D_J and z^3F_J states of Fe atoms in He and Ar. These excited states of Fe atoms can be easily formed by two-photon dissociation of Fe(CO)₅ followed by one-photon absorption within a laser pulse using an unfocused laser beam with atomic transition frequencies of Fe. The radiative lifetimes of z^3D_3 and z^3F_4 levels were obtained from kinetic simulations of the time profiles using three level kinetic scheme since the Stern–Volmer analysis of the decay frequencies gave an arithmetic mean value of the two levels due to strong collisional coupling between the levels. The radiative lifetimes of the higher-lying four levels were obtained directly from the pressure dependence of the decay frequencies. Collisional mixing among the higher-lying levels was also investigated by monitoring the time profiles of the laser excited and collisional product levels. State-to-state mixing rate constants were assigned from kinetic simulations of the time profiles. Although the state-to-state collisional branching fractions assigned in this work is based on the Fuhr and co-workers' Einstein A coefficients, it clearly shows that intermultiplet mixing is more efficient than intramultiplet mixing for this system.

ACKNOWLEDGMENTS

This work is financially supported in part by KOSEF through the Center for Molecular Science at KAIST and in part by the Ministry of Education through Basic Science Research Institute Program (BSRI-95-3438).

- ¹Z. Karny, R. Naaman, and R. N. Zare, *Chem. Phys. Lett.* **59**, 33 (1978).
- ²D. P. Gerrity, L. J. Rothberg, and V. Vaida, *Chem. Phys. Lett.* **74**, 1 (1980); *J. Phys. Chem.* **87**, 2222 (1983).
- ³G. W. Tyndall and R. L. Jackson, *J. Chem. Phys.* **89**, 1364 (1988).
- ⁴P. C. Engelking, *Chem. Phys. Lett.* **74**, 207 (1980).
- ⁵S. Leutwyler, U. Even, and J. Jortner, *Chem. Phys. Lett.* **74**, 11 (1980).
- ⁶S. A. Mitchell and P. A. Hackett, *J. Chem. Phys.* **79**, 4815 (1983); *Chem. Phys. Lett.* **107**, 508 (1984); *J. Chem. Phys.* **93**, 7813 (1990).
- ⁷K. Lee, J. S. Goo, and J. K. Ku, *Chem. Phys. Lett.* **244**, 213 (1995).
- ⁸J. R. Fuhr, G. A. Martin, and W. L. Wiese, *J. Phys. Chem. Ref. Data* **17**, Suppl. 4 (1988).
- ⁹K. Lee, J. S. Goo, and J. K. Ku, *Chem. Phys. Lett.* **216**, 483 (1993).
- ¹⁰J. T. Yardley, *Introduction to the Molecular Energy Transfer* (Academic, New York, 1980).
- ¹¹N. Sadeghi and D. W. Setser, *J. Chem. Phys.* **79**, 2710 (1983).
- ¹²S. C. Bae, K. Lee, G. H. Kim, and J. K. Ku, *J. Chem. Phys.* **102**, 1665 (1995).
- ¹³H. Figger, J. Heldt, K. Siomos, and H. Walther, *Astron. Astrophys.* **43**, 389 (1975).
- ¹⁴J. Marek, J. Richter, and H. J. Stanhke, *Phys. Scr.* **19**, 325 (1979).
- ¹⁵W. H. Breckenridge and H. Umemoto, *Adv. Chem. Phys.* **50**, 325 (1982).
- ¹⁶J. Elward-Berry and M. J. Berry, *J. Chem. Phys.* **72**, 4500 (1980).
- ¹⁷L. Krause, *Adv. Chem. Phys.* **28**, 267 (1975).
- ¹⁸C. B. Ke, S. H. Chou, K. C. Lin, and W. T. Luh, *J. Phys. Chem.* **97**, 604 (1993).
- ¹⁹K. C. Wang, K. C. Lin, and W. T. Luh, *J. Chem. Phys.* **96**, 349 (1992).
- ²⁰A. Spielfiedel, D. Gilvert, E. Roueff, and F. Lostas, *J. Phys. B* **12**, 3693 (1979).
- ²¹T. R. Mallory, W. Kedzierski, J. B. Atkins, and L. Krause, *Phys. Rev. A* **38**, 5917 (1988).
- ²²M. O. Hale and S. R. Leone, *J. Chem. Phys.* **79**, 3352 (1983).
- ²³J. F. Kelly, M. Harris, and A. Gallagher, *Phys. Rev. A* **37**, 2354 (1988).
- ²⁴N. P. Penkin and T. P. Redko, *Opt. Spectrosc.* **57**, 598 (1984).
- ²⁵H. Umemoto, T. Ohnuma, and A. Masaki, *Chem. Phys. Lett.* **171**, 357 (1990).
- ²⁶H. Umemoto, J. Kikuma, A. Masaki, T. Takayanagi, and S. Sato, *Chem. Phys.* **134**, 193 (1989).
- ²⁷H. Umemoto, A. Masaki, T. Ohnuma, T. Takayanagi, S. Sato, F. Misaizu, and K. Fuke, *J. Chem. Phys.* **93**, 4112 (1990).
- ²⁸X. L. Han and J. F. Kelly, *J. Chem. Phys.* **94**, 5481 (1991).
- ²⁹N. Bras, A. El Afghani, J. Butaux, J. C. Jeannot, and D. Perrin, *J. Chem. Phys.* **91**, 4142 (1989).
- ³⁰J. M. Parson and T. Ishikawa, *J. Chem. Phys.* **80**, 3137 (1984).